ANKARA YILDIRIM BEYAZIT UNIVERSITY

GRADUATE SCHOOL OF NATURAL AND APPLIED SCIENCES

EXPERIMENTAL AND THEORETICAL INVESTIGATION OF ENHANCED THERMOELECTRIC PERFORMANCE OF $GaAs_{1-x}N_x$ ALLOY WITH Si

M.Sc. Thesis by

Yusuf Yıldız

Department of Mechanical Engineering

April, 2018

ANKARA

EXPERIMENTAL AND THEORETICAL INVESTIGATION OF ENHANCED THERMOELECTRIC PERFORMANCE OF $GaAs_{1-x}N_x$ ALLOY WITH Si

A Thesis Submitted to

The Graduate School of Natural and Applied Sciences of

Ankara Yıldırım Beyazıt University

In Partial Fulfillment of the Requirements for the Degree of Master of Science in Mechanical Engineering, Department of Mechanical Engineering

by

Yusuf YILDIZ

April, 2018

ANKARA

M.Sc. THESIS EXAMINATION RESULT FORM

We have read the thesis entitled **"EXPERIMENTAL AND THEORETICAL INVESTIGATION OF ENHANCED THERMOELECTRIC PERFORMANCE OF $GaAs_{1-x}N_x$ ALLOY WITH Si"** completed by **YUSUF YILDIZ** under the supervision of **ASSIST. PROF. DR. KEMAL BİLEN** and we certify that in our opinion it is fully adequate, in scope and in quality, as a thesis for the degree of Master of Science.

Assist. Prof. Dr. Kemal BİLEN

Supervisor

Assoc. Prof. Yusuf ERDOĞDU

Jury Member

Prof. Dr. Cihangir DURAN

Jury Member

Prof. Dr. Fatih V. ÇELEBİ

Director

Graduate School of Natural and Applied Sciences

ETHICAL DECLARATION

I hereby declare that, in this thesis which has been prepared in accordance with the Thesis Writing Manual of Graduate School of Natural and Applied Sciences,

- All data, information and documents are obtained in the framework of academic and ethical rules.
- All information, documents and assessments are presented in accordance with scientific ethics and morals.
- All the materials that have been utilized are fully cited and referenced.
- No change has been made on the utilized materials.
- All the works presented are original.

11.04.2018 Yusuf YILDIZ

ACKNOWLEDGEMENTS

Firstly, I would like to express my deepest appreciation to all those who provided me the possibility to complete this thesis. A special gratitude I would like to give to my supervisor, Assist. Prof. Dr. Kemal BİLEN, who has contributed in my motivation by stimulating with suggestions and encouragement, helped me to coordinate my project especially by sharing with me his valuable experiences and knowledge.

Furthermore, I would also like to acknowledge with appreciation for the crucial role of the Prof. Dr. Abdullah YILDIZ, who has given the opportunities for utilizing all required sources and necessary material to research, as well as he has assisted for analyzing the results. A special thank goes to my team mate, Ph.D. Student Abdullah ATILGAN, who help me by giving information about the devices and their usage.

Many thanks go to the Italy, Mr. Matteo BOSI who has invested his full effort in preparing the samples and taking the necessary measurements of samples.

I would also like to thank Prof. Dr. Cihangir DURAN and Assoc. Prof. Yusuf ERDOĞDU for their valuable contributions and constructive criticisms during my thesis defense examination.

Finally, I must give voice to my heartfelt appreciations to my family, for supporting me in terms of incorporeal and corporeal throughout my all life and in the period of writing this thesis. This accomplishment would not have been possible without them.

Thank You…

2018, 11 April Yusuf YILDIZ

EXPERIMENTAL AND THEORETICAL INVESTIGATION OF ENHANCED THERMOELECTRIC PERFORMANCE OF $GaAs_{1-x}N_x$ ALLOY WITH Si

ABSTRACT

In this thesis, the application of un-doped and Si-doped gallium arsenide nitride ($GaAs_{1-x}N_x$) samples grown by Metal Organic Vapor Phase Epitaxy (MOVPE) technique on semi-insulating (SI) and *n*-type gallium arsenide (GaAs) substrates as a novel thermoelectric material was investigated.

Three different types of sample, which are fabricated in a horizontal MOVPE reactor by researcher Mr. Matte BOSI from Council of National Research (CNR) in Italy, have been included in this study.

X-Ray Diffraction (XRD) measurements for structural analysis, photoluminescence (PL) measurements for optical properties and Hall effect measurements for electrical results have been performed in Gazi University.

The Hall effect measurements were made as a function of temperature. The effects of layer structure and growth conditions of the samples on thermoelectric performance of $GaAs_{1-x}N_x$ were demonstrated by obtaining values of the power factor (*PF*).

Results show that Si doping has an affirmative influence on the *PF* value of $GaAs_{1-x}N_x$ when the samples are comprised to each other. It is found that the *PF* value of Si doped $GaAs_{1-x}N_x$ is approximately equal to ten times *PF* value of un-doped $GaAs_{1-x}N_x$. So that Si-doped $GaAs_{1-x}N_x$ might be considered as a promising candidate for thermoelectric energy harvesters.

Keywords: Thermoelectric, $GaAs_{1-x}N_x$, Si, Power factor, Seebeck effect, Peltier effect, Thomson effect.

Si KATKILI $GaAs_{1-x}N_x$ ALAŞIMININ İYİLEŞTİRİLMİŞ TERMOELEKTRİK PERFORMANSININ DENEYSEL VE TEORİK OLARAK İNCELENMESİ

ÖZ

Bu tezde; yarı iletken ve n-tipi GaAs altyapı taşları üzerine, metal organik buhar fazında epitaksi (MOVPE) yöntemi ile büyütülen Si katkılı ve katkısız $GaAs_{1-x}N_x$ numuneleri, yeni birer termoelektrik malzeme olarak çalışılmıştır.

Bu çalışmaya, İtalya'daki Uluslararası Araştırma Konseyi'nden (CNR) Araştırmacı Matteo BOSI tarafından yatay MOVPE reaktöründe üretilen, üç farklı numune dâhil edilmiştir.

Yapısal analiz için X-ışını saçınım (XRD) ölçümleri, optik özelliklerin incelenmesi için fotolüminesans (PL) ölçümleri ve elektriksel değerlerin belirlenmesi için ise Hall etkisi ölçümleri Gazi Üniversitesi'nde yapılmıştır.

Hall etkisi ölçümleri, sıcaklığın fonksiyonu olarak yapılmıştır. Katman yapısının ve numunelerin büyütülme şartlarının, $GaAs_{1-x}N_x$'in termoelektrik performansı üzerindeki etkisi, güç faktörü (*PF*) değerlerinin elde edilmesi ile gösterilmiştir.

Numuneler birbiri ile kıyaslandığında sonuçlar; Si katkısının $GaAs_{1-x}N_x$'in güç faktörü değeri üzerinde olumlu bir etkisinin olduğunu göstermektedir. Si katkılı $GaAs_{1-x}N_x$ numunesinin güç faktörü değerinin, katkısız $GaAs_{1-x}N_x$ numunesinin güç faktörü değerinin yaklaşık on katına eşit olduğu bulunmuştur. Bu yüzden, Si katkılı $GaAs_{1-x}N_x$, termoelektrik enerji üretimi için gelecek vaat eden bir malzeme olarak düşünülebilir.

Anahtar kelimeler: Termoelektrik, $GaAs_{1-x}N_x$, Si, Güç faktörü, Seebeck etkisi, Peltier etkisi, Thomson etkisi.

LIST OF TABLES

LIST OF FIGURES

NOMENCLATURE

Letter symbols

T	Absolute temperature, K
A	Area, cm^2
E_g	Band gap, eV
k_B	Boltzmann constant, $\frac{\mathrm{cm}^2 \cdot \mathrm{kg}}{\mathrm{s}^2 \cdot \mathrm{K}}$
n	Carrier concentration, cm^{-3}
e	Charge of electron, $1.602 \cdot 10^{-19}$ C
I	Current, A
J	Current flux, $\frac{\mathrm{A}}{\mathrm{cm}^2}$
R_H	Coefficient of hall
T_c	Cold temperature, K
m^*	Effective mass of carrier, kg
σ	Electrical conductivity, $\frac{1}{\Omega \cdot \mathrm{cm}}$
ρ	Electrical resistivity, $\Omega \cdot \mathrm{cm}$
E	Electrical field, $\frac{\mathrm{N}}{\mathrm{C}}$ or $\frac{\mathrm{V}}{\mathrm{m}}$
Z	Figure of merit, K^{-1}
q''	Heat flux, $\frac{\mathrm{W}}{\mathrm{m}^2}$
q, Q	Heat transfer rate, W
T_h	Hot temperature, K
L	Length, cm
R_L	Load resistance, Ω
L	Lorenz constant, $\frac{\mathrm{V}^2}{\mathrm{K}^2}$

B	Magnetic field, Gauss $\equiv \mathrm{cm}^3 \cdot \mathrm{C}^{-1}$
μ	Mobility, $\frac{\mathrm{cm}^2}{\mathrm{V \cdot s}}$
Π	Peltier coefficient, $\frac{\mathrm{W}}{\mathrm{A}}$ or V
ε_0	Permittivity of free space, $\frac{\mathrm{C}^2}{\mathrm{N \cdot m}^2}$
h	Planck constant, $\frac{\mathrm{cm}^2 \cdot \mathrm{kg}}{\mathrm{s}}$
R	Resistance, Ω
S	Seebeck coefficient, $\frac{\mu \cdot \mathrm{V}}{\mathrm{K}}$
ε_r	Static dielectric constant
k	Thermal conductivity, $\frac{\mathrm{W}}{\mathrm{cm \cdot K}}$
β	Thomson coefficient, $\mathrm{V} \cdot \mathrm{K}^{-1}$
GaAsN	Gallium Arsenide Nitride
CO_2	Carbon Dioxide
CH_4	Methane
N_2O	Nitrous Oxide
SF_6	Sulfur Hexafluoride
Bi_2Te_3	Bismuth Telluride
PbTe	Lead Telluride
SiGe	Silicon Germanium
BiSb	Bismuth-Antimony/Stibium
$Ca_3Co_4O_9$	Calcium Cobaltite
In_2O_3	Indium Oxide
$CaMnO_3$	Calcium Manganate
$SrTiO_3$	Strontium Titanate

La	Lanthanum
Nb	Niobium
∇T	Temperature gradient
Δ	Difference

Acronyms

a.u.	Arbitrary Unit
W_{com}	Compressor Work, W
EMF	Electromotive Force
ICT	Information and Communication Technology
MBE	Molecular Beam Epitaxy
MOVPE	Molecular Vapor Phase Epitaxy
NW	Nanowire
1-D	One-dimensional
PL	Photoluminescence
PF	Power Factor, $\frac{\mu w}{m \cdot K^2}$
SC	Semiconductor
SCCM	Standard Cubic Centimeters per Minute
TE	Thermoelectric
Wz	Wurtzite
W_t	Work Done by Turbine, W
XRD	X-Ray Diffraction
Zb	Zinc Blende

CONTENTS

CHAPTER 1

INTRODUCTION

1.1 Aim of the Thesis and a Brief View to Chapters

The main target of this study is to develop the performance of $GaAs_{1-x}N_x$ by changing the growth conditions and layer structure as well as doping with Si. A dimensionless figure of merit (ZT) is defined as an indicator of the thermoelectric performance, $ZT = (S^2\sigma/k)T$. Conceptually, to obtain a high ZT, both Seebeck coefficient (S) and electrical conductivity (σ) must be high, while thermal conductivity (k) must be decreased in this formula.

Because of the difficulty of measuring thermal conductivity (k), we have been concentrated on improving the power factor (PF) which can defined as $S^2\sigma$. By taking into account the results that are attained in the laboratory and theoretical information, PF values have been calculated. The conspicuous effect of silicon on improving of PF value of $GaAs_{1-x}N_x$ alloy has been observed in this study.

In the first chapter of this master thesis, general information has been given about energy and thermoelectric devices. In the second chapter, background of thermoelectricity and thermodynamic concept has been expressed with the theorems. In the third chapter; equipment used in the experiments, preparation of the samples, and experimental studies have been clarified. Obtained values from the measurements have been demonstrated with graphs and charts in the chapter four. In the last chapter, the results have been interpreted and discussed by considering obtained data.

1.2 A General View of Energy Sources and Clean Energy

Currently and close future, one of the most important issues in the world is the clean and eco-friendly energy. Inasmuch as; fossil fuels, that releases venomous greenhouse gases, are used so commonly in the world. Because of the detrimental

greenhouse gases like CO_2, CH_4, N_2O, SF_6 etc… natural life is coming across with global warming and climate change threat.

As it has been known that fossil fuels are base energy source; they have consistently been used in vehicle engines and heating system for various purposes. If we take into consideration that fossil fuels are running out and procurement of them is getting substantially hard, for overcoming this problem we need to find alternative energy technologies that are innocuous, renewable and fairly efficient. For obtaining higher efficiency, we must recover the "waste" energy, which has been released to environment after a process, and convert into useful energy. The "waste" energy is the energy that emanates from generators, thermal energy, vibration, heat engine, moving parts or moving fluids etc.

1.3 Thermoelectric Energy

Thermoelectric (TE) devices are appealing nominees for clean energy field because they can convert the heat energy (from temperature difference) into electrical energy without any emission of greenhouse gases. Moreover, they can fulfill cooling process by the reverse working system, when an electrical current is applied, temperature gradient will be generated which causes the temperature difference. One of the foremost advantages of TE devices is that they can execute cooling process without any moving parts as pump or turbine. Additionally, thermoelectric system is an environment-friendly energy conversion technology with the advantages of small size, high reliability, no pollutants and feasibility in a wide temperature range. On the other hand, the capability of cooling and generating energy is low if it is compared with other thermo cycles.

Nonetheless, thermoelectric devices have an important place in boosting the efficiency of energy technology by decreasing the energy consumption. As known; approximately 60% of generated energy in heat engine is lost as waste heat in the course of energy conversion process. Especially; in the vehicles, 80% of the energy that is produced by combustion reaction of the fuel-oil is loss. Inside of this loss energy, just about 20% of energy is used to drive the automobiles. Among this loss part of energy (80% of initial energy); nearly 60% is a waste heat, 30% exhaust loss

and 30% loss in radiator. The remaining parts of this loss energy are in friction and alternator. If TE devices are used to capture this waste energy and can turn into beneficial electricity then oil and coal consumption can be mitigated [1, 2].

TE devices have been used in cooling applications; for example microelectronic cooling in X-ray astronomy or microelectronics that need to operate in low temperature. In generating electrical energy for automobiles by accumulating waste energy from exhaust gases, in sensor applications, in temperature or water condensing sensors etc. Also; Peltier coolers can be used as a cooler in automotive seats and small consumer refrigerators, with their ability both heating and cooling. A dimensionless figure of merit (ZT) is defined as an indicator of the thermoelectric performance, $ZT = (S^2\sigma/k)T$. Conceptually, to obtain a high ZT, both Seebeck coefficient (S) and electrical conductivity (σ) must be large, while thermal conductivity (k) must be minimized so that the temperature difference producing Seebeck coefficient (S) can be maintained [1, 3].

The thermoelectric semiconductor materials most often used in today's TE coolers is an alloy of Bismuth Telluride (Bi_2Te_3). In addition to Bi_2Te_3, there are other thermoelectric materials including Lead Telluride (PbTe), Silicon Germanium (SiGe), and Bismuth-Antimony/Stibium (BiSb) alloys that may be used in specific situations.

In this thesis, we concentrated on the GaAsN semiconductor material, which is a compound of the elements gallium, arsenic and nitrate. Superior properties of GaAs are compelling reasons to use GaAs circuitry in mobile phones, satellite communications, microwave point-to-point links and higher frequency radar systems.

1.4 Review of Related Works

Thermoelectric performance and other properties of GaAs as a thermoelectric material have been investigated by loads of researchers. There are great number of researches that have been performed about GaAs and GaAsN in the different types of

scope. The studies related with our work, can be summarized as below which are the most common to our study in terms of topic and processes.

A group of scientists, Hou, Q. R., Gu, B. F., Chen, Y. B. and He, Y. J., studied on enhancement of thermoelectric power factor of $MnSi_{1.7}$ films by Si addition and modulation doping. Silicon-added and modulation-doped higher manganese silicide (HMS, $MnSi_{1.7}$) films have been prepared on glass substrates by magnetron-sputtering of $MnSi_{1.85}$, Si, and Al targets. Silicon-addition and modulation-doping are used to enhance the Seebeck coefficient and reduce the electrical resistivity, respectively. It is found that the silicon-added $MnSi_{1.7}$ film has a larger Seebeck coefficient (S), but a higher electrical resistivity (ρ) as well. The silicon-added $MnSi_{1.7}$ layer in a modulation-doped structure Si: Al/$MnSi_{1.7}$/glass, however, has a higher energy barrier height, a larger Seebeck coefficient, and a lower electrical resistivity [4].

Also; a group of researchers, Yamaguchi, M., Paek, J. and Amano, H., studied on thermoelectric power measurement of catalyst-free Si-doped GaAs nanowires (NWs). For growth of samples on Si substrate, they used the Molecular Beam Epitaxy (MBE) method. The electrical characteristics of the GaAs NWs were measured. A joule heater was arranged near the tip of NW for making the gradient of substrate temperature. They observed that obtained Seebeck coefficient of the GaAs NWs increases linearly with a rise in temperature [5].

Another scientists group, Zou, X., Chen, X., Huang, H., Xu, Y. and Duan, W. studied on enhanced thermoelectric figure of merit in thin GaAs NWs. Combining density functional theory and the non-equilibrium Green's function method, they investigated thermoelectric properties of thin GaAs nanowires (NWs). After identifying most-stable structures for GaAs NWs, either in wurtzite (wz) or zinc blende (zb) stacking, they presented a systematic analysis on the thermoelectric properties of these NWs and their dependence on stacking type (wz or zb), size of NWs, and temperature. Although bulk GaAs is a well-known poor thermoelectric material, the thermoelectric figure of merit ZT is significantly enhanced in thin GaAs NWs.

Adopting their unique electronic characteristics further enhancement is possible through surface engineering as introducing surface roughness or dopants [6].

Researcher Reshak, A.H., studied on thermoelectric properties of highly-mismatched alloys of GaN_xAs_{1-x} from first to second principles methods: energy conversion. The transport properties of GaN_xAs_{1-x} (x=0.0, 0.25, 0.5, 0.75 and 1.0) alloys are investigated using the semi-classical Boltzmann theory. Zunger approach was used to generate the structures of the GaN_xAs_{1-x} alloys. The carrier concentration (n), electrical conductivity (σ), Seebeck coefficient (S), thermal conductivity (k) and the electronic power factor (PF), as a function of temperature were obtained for GaN_xAs_{1-x} alloys. It has been found that GaN_xAs_{1-x} alloys show good transport properties, therefore, we expect that these alloys could be possible potential candidates for clean energy applications [7].

Scientists group Ohta S., Nomura T., Ohta H and Koumoto K. studied on high temperature carrier transport and thermoelectric properties of heavily La or Nb doped $SrTiO_3$ single crystals. Electron and thermal transport properties; electrical conductivity, carrier concentration, Hall mobility, Seebeck coefficient, thermal conductivity, of heavily La or Nb doped $SrTiO_3$ (STO) bulk single crystals were measured at high temperatures (300–1050 K). The influence of doping upon the thermoelectric performance of STO, was studied. Bulk single-crystal samples of La–STO or Nb–STO had been grown by a conventional Verneuil method at 2080 °C. The density of states effective mass of Nb-doped STO, which was estimated from the carrier concentration and Seebeck coefficient, was larger than that of La-doped STO. Thermal conductivity of the samples, which was similar to that of un-doped STO single crystal, decreased proportionally to T^{-1}, indicating that the phonon conduction takes place predominantly and the electronic contribution to thermal conductivity is negligible [8].

CHAPTER 2

BACKGROUND

2.1 Fundamentals of Thermoelectricity

For evolving and obtaining high efficiency TE devices, it is significant to understand the mechanism of TE devices which is basically related to three important effects; Seebeck, Peltier and Thomson effects.

2.1.1 Seebeck effect

An Estonian scientist Thomas Johann Seebeck discovered that the magnetic field between the two distinct metals was produced when junctions were held at the different temperatures, in 1821. After that, he realized that he had misunderstood when the Ampere's law was proposed around 1823. Instead of generating magnetism, it produces an electromotive force (EMF) or voltage between the dissimilar metals which can drive an electric current in a closed circuit [1]. This effect is stated as Seebeck effect, which is illustrated in the Figure 2.1 as a basic circuit and also given in Figure 2.2 as a general view of a thermoelectric generator.

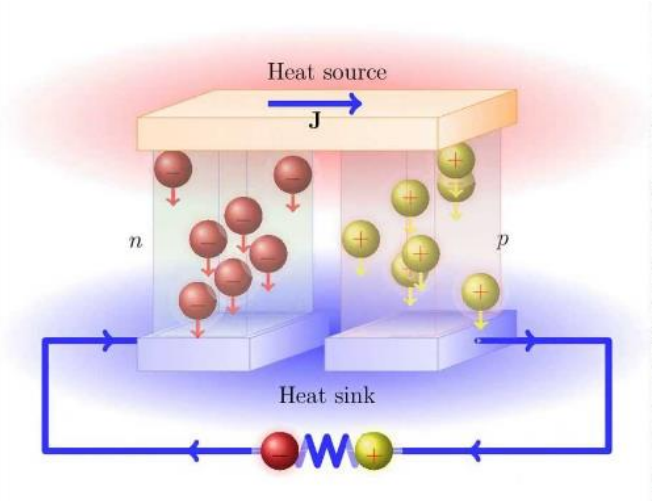

Figure 2.1 Typical demonstration of the Seebeck effect [9].

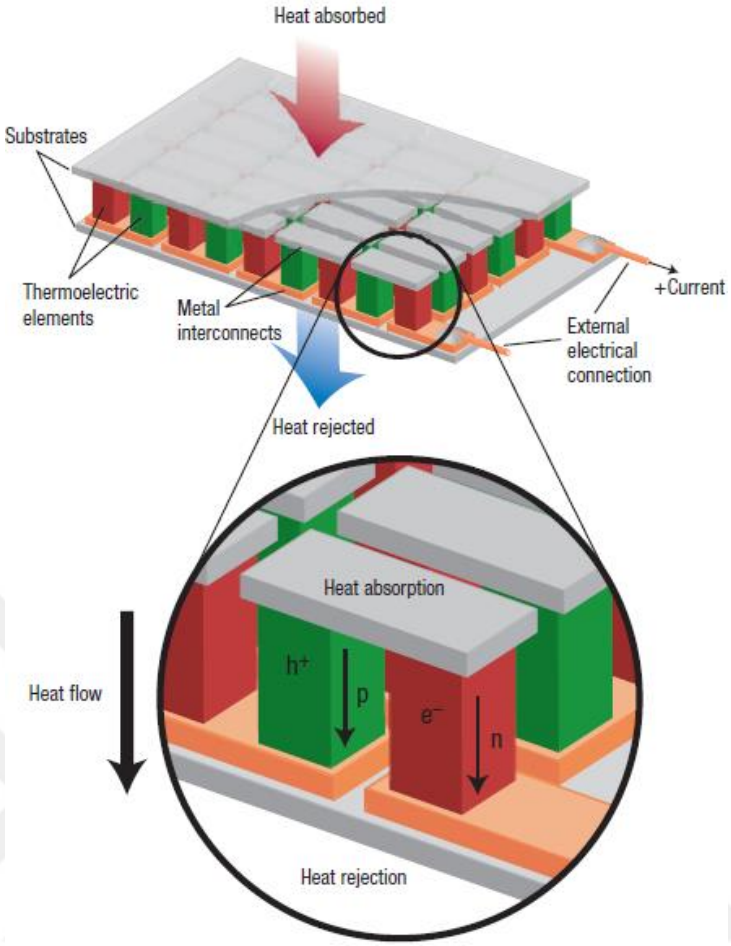

Figure 2.2 General view of the thermoelectric generator [10].

According to Seebeck effect, the voltage is proportional with the temperature difference and also it changes for different materials. Then it can be stated as in Equation (2.1);

$$\Delta V = (S_B - S_A)(T_H - T_C) = S_{AB}\Delta T \quad \textbf{(2.1)}$$

Where $S_{AB} = S_B - S_A$ is the difference of Seebeck coefficients of materials A and B ($\mu V \cdot K^{-1}$), V is thermoelectric voltage, and $\Delta T = T_H - T_C$ (K), is the difference of temperature between hot end and cold ends. If the temperature difference ΔT between the two ends of a material is small, then S can be expressed as in Equation 2.2;

$$S = \frac{\Delta V}{\Delta T} \quad \textbf{(2.2)}$$

2.1.2 Peltier effect

The second thermoelectric effect is Peltier effect which was discovered by Jean-Charles Peltier, in 1834. He proved that cooling occurs when electrical current flows through a thermocouple.

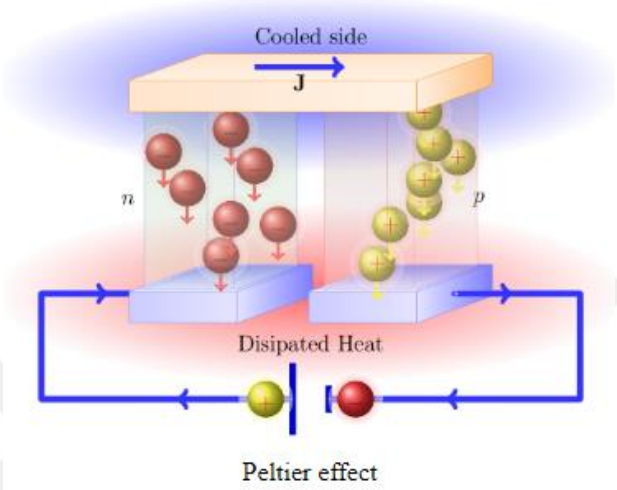

Figure 2.3 Typical demonstration of the Peltier effect [9].

On the other hand, the effect of heating occurs if electrical current is applied inversely. In 1838, Lenz verified the discovery of Peltier and demonstrated that the heating or cooling effect is related with the direction of current as seen in Figure 2.3. The rate of cooling q, at a junction of AB when a current I is applied from material A to material B, can be attain by the formula 2.3;

$$q = (\Pi_B - \Pi_A)I = \Pi_{AB} I \qquad \textbf{(2.3)}$$

where $\Pi_{AB} = \Pi_B - \Pi_A$ is the difference Peltier coefficients of materials the units of A and B is $(\frac{W}{A})$. The Peltier effect, however, is fairly difficult to determine experimentally because of Joule heating effect, which happens when current is flowed through a material [1].

2.1.3 Thomson effect

The connection between the Seebeck and Peltier effects were defined by William Thomson, who studied by using of thermodynamics laws, in 1855. Thomson concentrated on cooling rate of a system experimentally, by implementing a current

to a conductor which has a temperature difference between the two sides as shown in Figure 2.4. This effect is stated Thomson effect, which is admitted as the third thermoelectric effect. The heating or cooling is q as described in Equation 2.4;

$$q = \beta I \Delta T \tag{2.4}$$

where β can be stated as coefficient of Thomson of material in unit ($V \cdot K^{-1}$), I is the current which passes along the materials, ΔT is the temperature difference. The heating or cooling cases are related with electrical discharge of material, which results in positive Thomson coefficient ($+\beta$) or negative Thomson coefficient ($-\beta$). The effect of Thomson shows the basic linkage between Seebeck and Peltier coefficients [11].

Thomson noticed that the Seebeck coefficient changes with temperature and the gradient of the heat flux is then given by the relations 2.5 and 2.6;

$$\beta = \frac{dS}{dT} T \tag{2.5}$$

$$\frac{dQ}{dx} = \beta I \frac{dT}{dx} \tag{2.6}$$

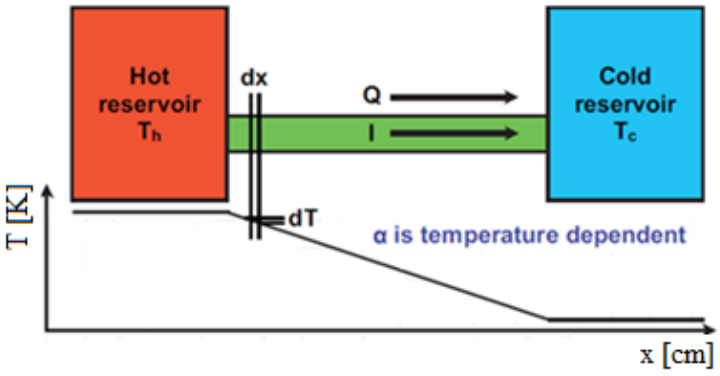

Figure 2.4 Change of the Seebeck coefficient with temperature [11].

After solving the Equations 2.5 and 2.6 the relation between Peltier and Seebeck coefficient can be stated as below in Equation 2.7;

$$\Pi = ST \tag{2.7}$$

Experimentally, measuring of the Peltier and Thomson coefficients are fairly difficult. On the other hand, Seebeck coefficient is easier to calculate because it only needs a voltage difference measurement as a function of ΔT through the thermoelectric material.

2.2 Basic Concepts of Thermodynamic

2.2.1 Joule's first law and Fourier's heat conduction law

For deriving the thermoelectric efficiency we can firstly use Joule's heating law effect. Joule discovered that heat is produced through a resistor in case of passing a current. In particular; the heat, Q generated by a flowing current, I along a resistance, R can be expressed by Joule's first law in Equation 2.8;

$$Q = I^2 R \tag{2.8}$$

It is known that the generated heat by a process will be transmitted in a material via the temperature gradients along the material as shown in Figure 2.5 [11].

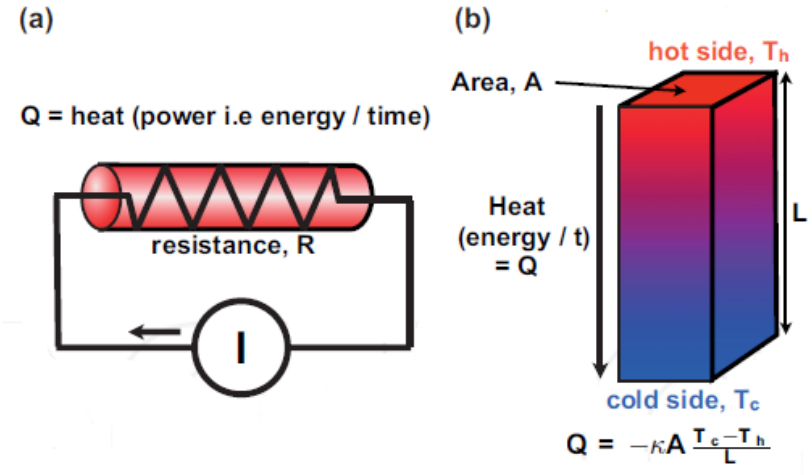

Figure 2.5 Joule's first law and Fourier's heat conduction law [11].

This can be explained by Fourier's law of heat transport in Equation 2.9 for a material with area A and thermal conductivity k that;

$$Q = -kA\nabla T = -\frac{kA(T_c - T_h)}{L} \text{ (for 1 dimensional trasport along length L)} \tag{2.9}$$

Actually, the heat transport could be in multiple directions in a complex material with a range of different thermal conductivities in different directions. For the most thermoelectric systems, the designs are in the trend of making the heat flow easy by using 1-D constructs [11].

2.2.2 Thermodynamic efficiency

In this section the relation and similarity of thermo dynamical efficiency of Carnot cycle have been presented, with respect to thermoelectric efficiency of thermoelectric materials. Thermoelectric efficiency of thermoelectric materials was first demonstrated by Altenkirch in 1909-1911. So that, for understanding this phenomenon we can investigate the Carnot cycle which has the maximum efficiency in terms of converting a given heat energy, into turbine work. Therefore, topics related with the maximum efficiency for any thermal system and how much the efficiency can be improved, may be interpreted for improving thermoelectric materials.

Figure 2.6 demonstrates the classical Carnot cycle where W_{com} is the input work performed by a compressor for raising the water pressure. This input work process is adiabatic so that there is no loss or gain of energy in the system. As seen in Figure 2.6, the water passes from the compressor to a furnace for gaining an amount of heat Q_1, at constant temperature. In the furnace, the water is converted into vapor phase along an isotherm. Thus, all the heat energy gained from furnace during this process is the latent heat for changing water into dry steam.

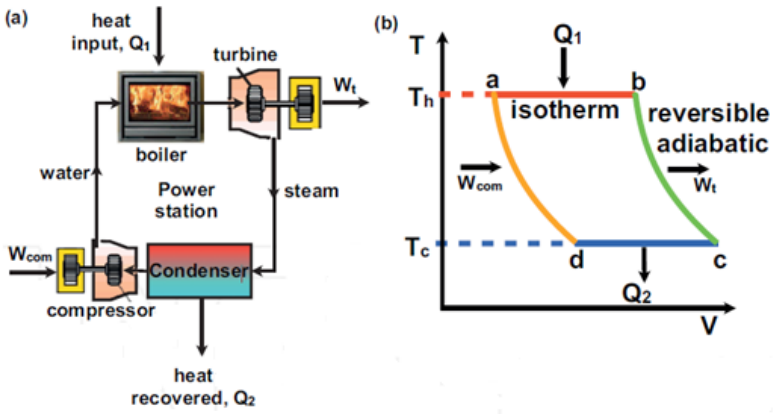

Figure 2.6 Sketch and *T*-*V* diagram of Carnot cycle [11].

The steam volume is larger than the water volume and so there is an increase of volume in the system as shown in Figure 2.6 (b). This increase in the volume can be used to turn a turbine and the kinetic energy from the volume expansion can be recovered as work done on the turbine, W_t. The temperature is reduced in this process. Then to allow the cycle to start again, the steam has to be condensed into water and the latent heat Q_2 removed at constant temperature in the condenser. So that, this condensed steam can be recovered and reused as input water in compressor. The process can then start again [11].

We can give the Carnot cycle efficiency as below in Equation 2.10;

$$\text{Efficiency} = \eta = \frac{\text{Net work output}}{\text{Net work input}} = \frac{W_t - W_{com}}{Q_1} \quad \textbf{(2.10)}$$

From the first law of thermodynamics (energy conservation), we have Equation 2.11;

$$(Q_1 - Q_2) - (W_t - W_{com}) = 0 \quad \textbf{(2.11)}$$

And by using Equations 2.10 and 2.11 then efficiency can obtained as in Equation 2.12;

$$\eta = \frac{Q_1 - Q_2}{Q_1} = 1 - \frac{Q_2}{Q_1} \quad \textbf{(2.12)}$$

By using the diagram of temperature versus volume, Carnot indicated that maximum efficiency of Carnot cycle is only related to the maximum (T_h) and minimum temperatures (T_c) in the cycle in K unit and so the maximum efficiency can be expressed as in Equation 2.13;

$$\eta_c = 1 - \frac{T_c}{T_h} \quad \textbf{(2.13)}$$

The Carnot efficiency is related with the second law of thermodynamic which defines that any system or equipment cannot convert the all gained energy, into same amount of work. Briefly, it can be expressed that no thermodynamic system is available having 100% efficiency.

Heat flow is always in the direction of from a hotter environment to a colder environment. Heat energy can be moved from a colder environment to a hotter environment by making work on the system. So that, as known in Peltier effect, if a current is applied to system heat energy can be moved from colder environment to a hotter environment.

The Equation 2.13 basically represents that the efficiency of the system can be raised by diminishing T_c or increasing T_h. In other words; the larger value of temperature difference $\Delta T = T_h - T_c$ results, the higher the efficiency. For this reason; in practical systems, the simple manner for boosting the efficiency of any system is to raise the temperature of hot reservoir T_h.

2.2.3 Thermoelectric efficiency and figure of merit (ZT)

It has been explained above how a temperature difference across a material causes heat conduction in accordance with the law of Fourier if electrical current does not pass in the system. In addition to this heat conduction; if there is an electrical current owing to the Seebeck effect then the Peltier effect will act in the opposite direction of exerted temperature gradient. So that, if the heat moves along a TE material between hot and cold sides, it must be considered not only the Fourier' s heat conduction phenomenon but also the effect Peltier.

We therefore need to write: Heat flux per unit area = Peltier term + Fourier term as in Equation 2.14;

$$\frac{Q}{A} = \Pi J - k\nabla T, \qquad JA = I \tag{2.14}$$

From the Equation 2.7 we have $\Pi = ST$ and the current density. Therefore this can be rewritten as in Equation 2.15;

$$Q = SIT - kA\nabla T \tag{2.15}$$

For deriving the thermodynamic efficiency of thermoelectric generator, we should prepare an electrical cycle that can transmit the power to a load. Figure 2.7(a) illustrates the simple thermoelectric cycle for producing electricity which is

comprised of an n-type and a p-type semiconductor rods. The power, which is transmitted to a load, generated just in the resistor R_L. As a Peltier cooler, a similar electrical cycle can be devised that the load is replaced by a current supply or battery as illustrated in Figure 2.7(b).

The thermodynamic efficiency of the TE generator is stated by the Equation 2.16 below;

$$\eta = \frac{\text{power supplied to load}}{\text{heat absorbed at hot junction}} \tag{2.16}$$

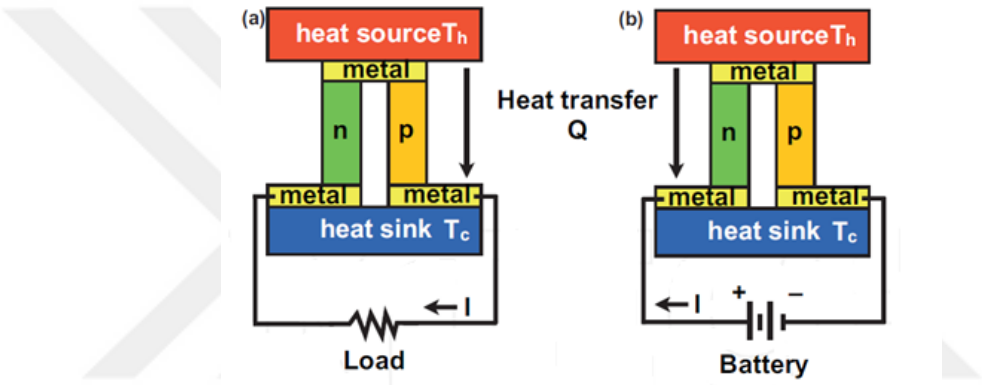

Figure 2.7 Thermoelectric generator and Peltier cooler [11].

The transmitted power to the load is only the Joule heating due to load resistor R_L which is equal to I^2R_L. The heat absorbed at the hot junction is the Peltier term plus the heat withdrawn from the hot junction as described above. The Peltier heat can be given as $\Pi I = SIT_h$. If the resistance of the n-type and p-type semiconductor elements in series is R, then the current I flowing in the circuit can be given by Ohm's Law as in Equation 2.17;

$$I = \left(\frac{\Delta V}{R_{total}}\right) = \frac{S(T_h - T_c)}{R + R_L} \tag{2.17}$$

The heat withdrawn from the hot junction Q_h is given by the Fourier term but as there will be Joule heating from the generated current from the Seebeck voltage. So that, some heat will also be generated and returned to the hot junction. It is usually

assumed that half of the Joule heat will be transport and half will be returned to the hot junction.

$$\mathrm{Q_h} = \text{Fourier} - \text{Joule heating} + \text{half joule heating returned}$$

$$= kA(T_h - T_c) - I^2R + \left(\frac{1}{2}\right)I^2R \quad \textbf{(2.18)}$$

$$= kA(T_h - T_c) - \left(\frac{1}{2}\right)I^2R \quad \textbf{(2.19)}$$

Now efficiency can be calculated as given in Equation 2.20 by putting in together these terms and supposing that the delivered power to the load is just owing to Joule heating.

$$\eta = \frac{Power\ supplied\ to\ load}{Heat\ absorbed\ at\ hot\ juntion} \quad \textbf{(2.20)}$$

$$\eta = \frac{\text{Power supplied to load}}{\text{Peltier+heat withdrawn from hot junction } (Q_h)} \quad \textbf{(2.21)}$$

$$\eta = \frac{I^2R_L}{\mathrm{SIT_h} + kA(T_h - T_c) - \left(\frac{1}{2}\right)I^2R} \quad \textbf{(2.22)}$$

To obtain the maximum efficiency, this equation needs to be solved for $\frac{d\eta}{d\left(\frac{R_L}{R}\right)} = 0$

The ratio of $\frac{R_L}{R}$ is equal to *M* which is defined as below Equation 2.23 by Ioffe [12]

$$M = \frac{R_L}{R} = (1 + ZT)^{0.5} \quad \textbf{(2.23)}$$

By solving this equation it can be shown that the maximum efficiency can be obtained as in Equation 2.24;

$$\eta_{\max} = \left(1 - \frac{\mathrm{T_c}}{\mathrm{T_h}}\right)\frac{(1+\mathrm{ZT})^{0.5} - 1}{(1+\mathrm{ZT})^{0.5} + \frac{\mathrm{T_c}}{\mathrm{T_h}}} \quad \textbf{(2.24)}$$

where $\mathrm{T} = \frac{1}{2}(\mathrm{T_h} + \mathrm{T_c})$ and the figure of merit for TEs is defined as in Equation 2.25;

$$ZT = \frac{\mathrm{S}^2\sigma}{\mathrm{k}}T \quad \textbf{(2.25)}$$

where the term in Equation 2.25 can be defined as;

Z: Figure of merit, K^{-1}

S: Seebeck coefficient, $\frac{\mu\cdot\mathrm{V}}{\mathrm{K}}$

σ: Electrical conductivity, $\frac{1}{\Omega\cdot\mathrm{cm}}$

k: Thermal conductivity, $\frac{\mathrm{W}}{\mathrm{cm}\cdot\mathrm{K}}$

T: Absolute temperature, K

The single *ZT* value states that the thermoelectric efficiency of materials requires enhanced Seebeck coefficient, electrical conductivity, and small values of thermal conductivity. On the other hand, measuring thermal conductivity of thin film samples is quite arduous. Inasmuch as slim film (approximately hundreds of nanometer thick) samples have to be produced on a substrate, the thermal conductivity of substrate will be more effective over the heat flow. So that, a stable temperature gradient along the slim film sample structure cannot be attained. Because of the difficulty of measuring thermal conductivity (*k*), we can concentrate on improving the power factor (*PF*) which can define as below [2].

$$PF = S^2\sigma \tag{2.26}$$

2.2.4 Electrical conductivity

In this study, $GaAs_{1-x}N_x$ as a semiconductor material was investigated. The number of free electrons in semiconductors; is generally among the number of free electrons in insulator and conductor. At the temperatures of absolute zero; a semiconductor crystal acts as an insulator because there are no free electron/hole carriers to conduct the electricity. On the other hand; at room temperature (300 K) some of the covalent bond structures in the crystal are broken by force of available energy. This event causes the increasing number of free electrons in the crystal and herewith conduction of semiconductor may be possible at room temperature.

If one of the covalent bonds is broken, electrons that are previously included in the bond formation will emerge by leaving an empty place behind it on the bond. This empty place is called as a hole. When an electron moves to fill this hole by leaving

its previous position, it will leave another new hole behind it. When the second hole is generated, then electron of other adjacent bond can come to fill up the second hole by leaving a new hole behind it. Therefore, it can be explained that these holes are moving in the opposite direction of the electrons [13].

Considering above explanation; it can be stated that electrons and holes move at the same time in opposite direction. If the temperature goes up the quantity of electron-hole pair generation raises and when the temperature reduces, the concentration of electron-hole pairs will decrease again because of recombination of holes and electrons in the crystal. When one electron-hole pair is produced, there will be two charge carriers. One of them is negative charge carrier related to electron and other is positive charge carrier related with the hole. Mobility of the hole in the crystal is $\mu_h$and the mobility of electron in the same crystal is μ_e. These holes and electrons move in opposite direction. The electrons always tend to move in opposite to the applied electric field,

The current density due to drift of holes is given by the Equation 2.27;

$$J_h = epv_h = ep\mu_h E \tag{2.27}$$

The current density due to drift of electrons is given by the Equation 2.28;

$$J_e = env_e = en\mu_e E \tag{2.28}$$

n: The magnitude of free electron concentration, cm^{-3}

p: The magnitude of holes concentration, cm^{-3}

μ_h: Mobility of the holes, $\frac{\mathrm{cm}^2}{\mathrm{V{\cdot}s}}$

μ_e: Mobility of the electrons, $\frac{\mathrm{cm}^2}{\mathrm{V{\cdot}s}}$

e : Charge of electron, $1.602 \cdot 10^{-19}$ C

v_e: Velocity of electron, $\frac{\mathrm{m}}{\mathrm{s}}$

v_h: Velocity of hole, $\frac{\mathrm{m}}{\mathrm{s}}$

E : Electric field, $\frac{\mathrm{N}}{\mathrm{C}}$ or $\frac{\mathrm{V}}{\mathrm{m}}$

Hence, resultant current due to these both charge carriers will be sum of two currents and hence resultant current density is stated as in Equations 2.29 and 2.30;

$$J = J_h + J_e = epv_h + env_e = ep\mu_h E + en\mu_e E = (p\mu_h + n\mu_e)eE = \sigma E \quad \textbf{(2.29)}$$

$$ep\mu_h + en\mu_e = \sigma \quad \textbf{(2.30)}$$

2.2.5 Thermal conductivity

It is well known that metals are good conductors of heat as we know from our daily life experiences. For example; we can't handle a metal spoon easily which is exposed a hot tea for a long time. On the contrary, most non-metals, such as plastics and glass, are feeble thermal conductors as they are poor electrical conductor.

For metals, the thermal conductivity is quite high, and those metals which are the best electrical conductors are also the best thermal conductors. At a given temperature, the thermal and electrical conductivities of metals are proportional, but raising the temperature increases the thermal conductivity while decreasing the electrical conductivity. This behavior is quantified in the Wiedemann-Franz Law as below in Equation 2.3;

$$\frac{k}{\sigma} = LT \quad \textbf{(2.31)}$$

L: Lorenz constant, $\frac{\mathrm{V}^2}{\mathrm{K}^2}$

k: Thermal conductivity, $\frac{\mathrm{W}}{\mathrm{cm \cdot K}}$

σ: Electrical conductivity, $\frac{1}{\Omega \cdot \mathrm{cm}}$

It is a prevalent idea that the movement of electrons contribute to thermal conduction if we take into consideration the compatible relationship between thermal and electrical conduction. On the other hand, if we consider a diamond, it is found to be perfect thermal conductor, despite the fact that they are electrical insulators. This suggests that there must be some process other than the transport of electrons which contributes to thermal conduction.

This process is the vibration of the atoms that come into by heating of materials. Since the bonds between the atoms behave like springs, the increase in amplitude of vibration of one atom affects the vibration of the neighboring atom. Therefore, heat energy is transferred by thermal waves travelling through the material. So, it can also be called these thermal waves as particles, phonons. Similar to this term, we can also denominate the light waves in terms of photons [14].

Conversely to electrical conduction, which is purely due to the movement of electrons, we find that thermal conduction involves two types of particles; electrons and phonons. The total thermal conductivity can be written as in Equation 2.32;

$$k = k_e + k_p \tag{2.32}$$

2.2.6 Thermoelectric materials

a) Ceramics: A ceramic is an inorganic non-metallic solid made up of either metal or non-metal compounds that have been shaped and then hardened by heating to high temperatures. In general, they are hard, corrosion-resistant and brittle. Generally, ceramic materials are used as thermoelectric devices; for high temperature applications like gas burners, combustion engines, nuclear fuel, or furnaces. Metal oxides ($Ca_3Co_4O_9$, $CaMnO_3$, $SrTiO_3$, In_2O_3), Ti sulfides, and Mn-silicides are promising TE (thermoelectric) material candidates for cascade-type modules that are usable in a temperature range of 300–1200 K in air [15-17].

b) Polymers: Polymers are very large molecules that are made up thousands, even millions of atoms that are bonded together in a repeating pattern. Conducting polymers have several attractive features for use as TE elements. They are lightweight, flexible, and cheap. However, they are associated with a major disadvantage of poor efficiency, that is, a relatively low ZT. The improvement of the electrical conductivity of these polymers can be achieved by doping the polymer with a sufficient quantity of a suitable doping agent. Conjugated semiconducting polymers, such as poly-acetylene, poly-pyrroles, poly-anilines, poly-thiophenes, poly-carbazoles and so on, have been studied for their TE applications.

More recently, conjugated polymers such as poly-acetylene and poly-ethylenedioxythiophene show a unique opportunity in TEs, based on reports showing that their efficiency in converting temperature differences to electrical potentials. They have been extensively studied for their applications as light-emitting diodes, transistors, sensors, and photovoltaic cells [18].

c) Semiconductors: A material product, usually comprised of silicon, which conducts electricity more than an insulator but less than a pure conductor as copper and aluminum, can be defined as semiconductor. They are quite common, found in almost all electronic devices. Good examples of semiconductor materials can be given as Ge, GaAs, and Si. There are two types of semiconductors according to their material composition.

Intrinsic semiconductors; are composed of only one kind of material. Extrinsic semiconductors; are made of intrinsic semiconductors that have had other substances added to them to alter their properties (they have been doped with another element).

There are two types of extrinsic semiconductors: p-type (p for positive: a hole has been added through doping with a group-III element) and n-type (n for negative: an extra electron has been added through doping with a group-V element).

A semiconductor is a crystal material whose ability to conduct electricity rises as its temperature goes up. That is, it sometimes acts as a conductor and sometimes as an insulator. Its conducting ability can be much increased by chemical treatment [19].

2.2.7 Discussion of thermoelectric materials

The first question arises what class of materials can be potential as thermoelectric materials? The comparison of thermoelectric properties of metals, semiconductors and insulators at 300 K is shown in Table 2.1.

It is clear that metals have very good electrical conductivity value ($\sim 10^{6} \Omega^{-1} \mathrm{cm}^{-1}$) if they are compared with other materials in the same conditions. However, their very low Seebeck coefficient ($\sim 5\ \mu \mathrm{V} \cdot \mathrm{K}^{-1}$) and large thermal

conductivity do not make them desirable materials for thermoelectric applications. For insulators with large band gap, although they have large Seebeck coefficient ($\sim 1000 \mu V \cdot K^{-1}$), their extremely low electrical conductivity ($\sim 10^{-12} \Omega^{-1} cm^{-1}$) results in a small value of *PF*, and thus a small Z($\sim 5x10^{-17} K^{-1}$), which is far smaller than that of metal ($\sim 3x10^{-6} K^{-1}$) . The optimal thermoelectric material with a large value of *Z* is located in the region of semiconductor as seen in Table 2.1 [20].

Table 2.1 TE properties of metals, SCs and insulators at room temperature [20].

Property	**Metals**	**Semiconductors**	**Insulators**
$\boldsymbol{S}$ ($\mu V K^{-1}$)	~5	~200	~1000
$\boldsymbol{\sigma}$ ($\Omega^{-1} cm^{-1}$)	$\sim 10^{6}$	$\sim 10^{3}$	$\sim 10^{-12}$
$\boldsymbol{k}\left(\frac{W}{cm \cdot K}\right)$	$\sim 8.33 \cdot 10^{12}$	$\sim 2 \cdot 10^{10}$	$\sim 2 \cdot 10^{10}$
$\boldsymbol{Z}$ (K^{-1})	$\sim 3 \cdot 10^{-6}$	$\sim 2 \cdot 10^{-3}$	$\sim 5 \cdot 10^{-17}$

The insulators have the highest Seebeck coefficient if it is comprised with semiconductors and metals which have been illustrated in Figure 2.8. Even though this phenomenon seems favorable for boosting *PF* value of insulators, it is also known that insulators have too low electrical conductivity.

In the same way, if it comes to evaluating the *PF* value of the metals; it can be easily observed that metals have superior value of electrical conductivity. Nonetheless, it is also clear that Seebeck coefficient of them is quite poor as seen in Figure 2.8. So that, it can be inferred that the best thermoelectric materials which can be operated in room temperatures are semiconductors due to their high *PF* values [20].

2.2.8 Doping Process, degenerate and non-degenerate semiconductors

The conductivity of semiconductors may easily be modified by introducing impurities into their crystal lattice. The process of adding controlled impurities to a semiconductor is known as doping. The amount of impurity, or dopant, added to an intrinsic (pure) semiconductor varies its level of conductivity.

A degenerate semiconductor is a semiconductor with such a high level of doping that the material starts to act more like a metal than as a semiconductor. As seen from Figure 2.8 semiconductors with high amount of doping (degenerated), exhibit the best power factor among the others [21].

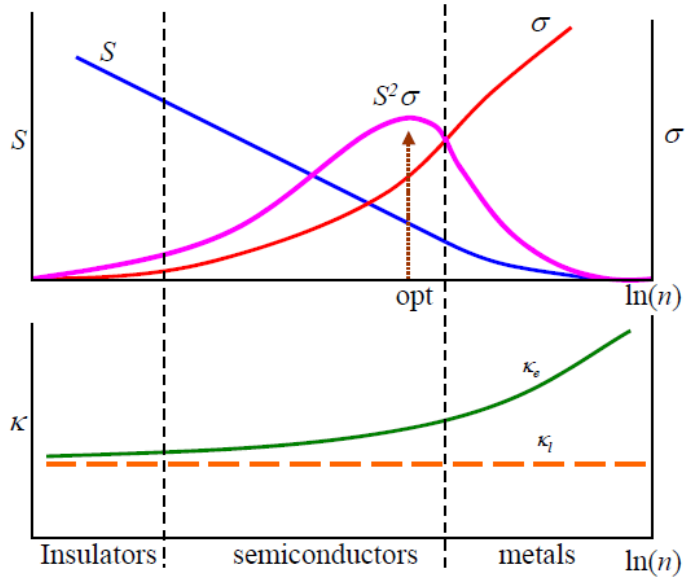

Figure 2.8 Optimum *PF* value of degenerated SC [20].

The quantity of dopant introduced to an intrinsic semiconductor determines its concentration and indirectly affects many of its electrical properties. The most important factor is that doping directly affects is the material's carrier concentration.

Carrier concentration: The number of electrons and holes that can participate in conduction.

Insulators with lower carrier concentration and even semiconductors have large Seebeck coefficients; see Equation (2.33). However, low carrier concentration also results in low electrical conductivity; see Equation (2.34). The interrelationship between carrier concentration and Seebeck coefficient can be seen from relatively simple models of electron transport [10].

For metals or degenerate semiconductors Seebeck coefficient is given by Equation 2.33;

$$S = \frac{(8\pi^2)(k_B^2)}{3eh^2} m^* T \left(\frac{\pi}{3n}\right)^{\frac{2}{3}} \quad \textbf{(2.33)}$$

where k_B is the Boltzmann constant, m^* is the effective mass of carrier, h is the Planck constant, n is the carrier concentration, e is the electron charge.

The electrical conductivity (σ) and electrical resistivity (ρ) are related to n through the carrier mobility μ:

$$\frac{1}{\rho} = \sigma = ne\mu \quad \textbf{(2.34)}$$

CHAPTER 3

EXPERIMENTS AND MEASUREMENTS

3.1 Growth Conditions and Sample Preparation of $GaAs_{1-x}N_x$

In this thesis three $GaAs_{1-x}N_x$ samples were grown by MOVPE technic by researcher Mr. Matte BOSI from CNR, in Italy. As seen Figure 3.1, MOVPE is an epitaxial crystal growth technique used for growing high quality single crystalline thin films of different materials on different substrates [22].

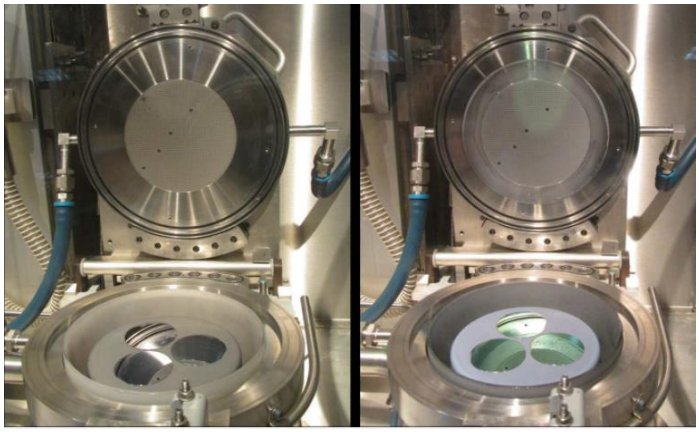

Figure 3.1 Sketch of MOVPE system for growth of samples [22].

As shown in Table 3.1, the samples were grown in a horizontal MOVPE reactor heated by infrared lamps, at pressure of 100 and 750 mmHg (Torr). Trimethylgallium (TMG), arsine (AsH_3) and dimethylhidrazine (DMHy) were used as Ga, As and N precursors, respectively, diluted in 2000 sccm (standard cubic centimeters per minute) palladium-purified H_2 carrier gas. $GaAs_{1-x}N_x$ layers have been deposited at 515-530 °C on a 50 nm-thick GaAs buffer layer grown at 600 °C.

Ga: $1s^2\ 2s^2\ 2p^6\ 3s^2\ 3p^6\ \mathbf{4s^2}\ 3d^{10}\ \mathbf{4p^1}$ (III-A)

As: $1s^2\ 2s^2\ 2p^6\ 3s^2\ 3p^6\ \mathbf{4s^2}\ 3d^{10}\ \mathbf{4p^3}$ (V-A)

N: $1s^2\ \mathbf{2s^2\ 2p^3}$ (V-A)

Si: $1s^2\ 2s^2\ 2p^6\ \mathbf{3s^2\ 3p^2}$ **(**IV-A)

Table 3.1 Growth parameters of examined samples.

Parameters	**Sample A**	**Sample B**	**Sample C**
Growth temperature (^{o}C)	530	515	515
Reactor pressure (Torr) (1 Torr = 133.322 Pa)	750	100	100

The layer structure of the samples is shown in Figure 3.2. The sample A is grown on 350 µm thick n-type (100) GaAs substrate, disoriented 2° off towards the [110] direction. The other samples (sample B and C) are grown on 450 µm thick semi-insulating (SI) (100) GaAs substrate. The thickness of the GaAsN layers is in the range 350 - 400 nm, depending from growth parameters. Sample C was doped n-type using a SiH_4 flow during the growth process.

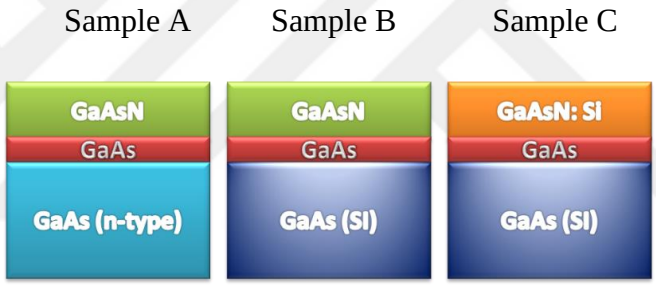

Figure 3.2 Illustration of the $GaAs_{1-x}N_x$ samples.

3.2 Structural Measurements

In this work, Lake Shore Hall effect measurement system was used which is available in the laboratory of Gazi University. For thin film analysis, XRD is one of the most common techniques to identify the epitaxial films structure of samples. XRD is used to detect the crystalline phases in a specimen; structural properties can be precisely specified as strain state, size of grain, epitaxy structure, orientation tendency and more.

Figure 3.3 Picture of Bruker D8 Discover XRD measurement device [23].

The XRD measurements were performed by a D8 Discover diffractometer shown in Figure 3.3 equipped on the primary side with a Ge (220) monochromator. To determine nitrogen concentration and thickness of the samples, the XRD data is simulated with software based on XRD. The simulation results fitted to the measurement are also shown in the Figure 3.4. The measurement and the simulation are in good agreement for the samples. Analysis of XRD data for the samples indicates the presence of two different crystalline phases. One peak which is about 33° corresponds to GaAs, while other one which is little away indicates $GaAs_{1-x}N_x$.

Applying linear Bragg and Vegard's law, the nitrogen composition (x) in the $GaAs_{1-x}N_x$ is determined. The values of x are obtained for samples A, B and C 2.98%, 3.01% and 2.91%, respectively. [24]

The position of $GaAs_{1-x}N_x$ peak depends on the average nitrogen concentration. As seen in Figure 3.4 the peaks for $GaAs_{1-x}N_x$ shifts to left side slightly, because of having different concentration of nitrogen.

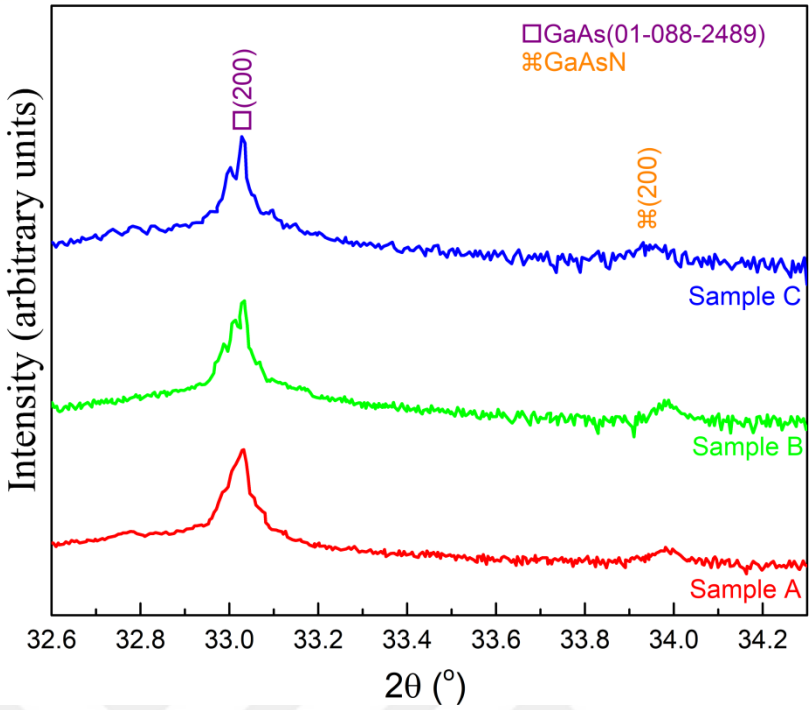

Figure 3.4 Results of XRD measurements.

3.3 Optical Measurements

Photoluminescence (PL) is light emission from any form of matter after the absorption of photons (electromagnetic radiation). In other words, we can also define as releasing electromagnetic radiation of a matter without changing its heat energy. It is one of many forms of luminescence (light emission) and is initiated by photo excitation (excitation by photons) as seen in Figure 3.5. Following excitation various relaxation processes, typically occur in which other photons are re-radiated.

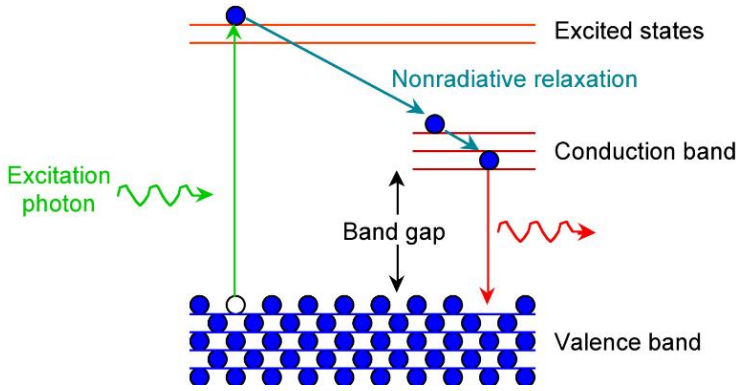

Figure 3.5 Illustration of photoluminescence phenomenon [25].

PL is a useful device for getting some ideas about imperfections and impurities in crystal structure. The main principle of the this device is; accumulating the light emission of a system that excited with an optical light source and obtaining spectrum in accordance with wave length or energy.

The main optical components of this instrument are: a lamp that provides the light used to excite the sample, two monochromators (M), one for the excitation (M_{ex}) and the other one for the emission (M_{em}) and a detector, usually a photomultiplier [26].

To determine band gap (E_g) values of the samples, the PL measurements were employed by Horiba Jobin Yvon Fluorolog-3 Laser as shown in Figure 3.6 at Gazi University.

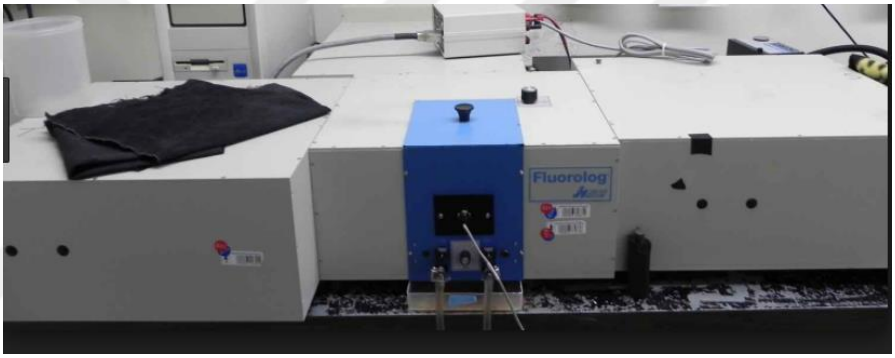

Figure 3.6 Horiba Jobin Yvon Fluorolog-3 Laser for PL measurements.

The band gap of the films is examined by PL measurements. Figure 3.7 shows the PL spectra of the samples. As more N is incorporated, the absorption edge slightly shifts to shorter wavelength, indicating an increase of the band-gap energy (E_g). An increase in the peak energy obtained from the PL spectra with increasing nitrogen concentration is negligible due to their similar nitrogen values. The values of E_g are found as 1.2701, 1.2703 and 1.2695 eV for sample A, B and C, respectively. The band gap values obtained from the PL measurements are of the same order of magnitude as found in variety systems [24].

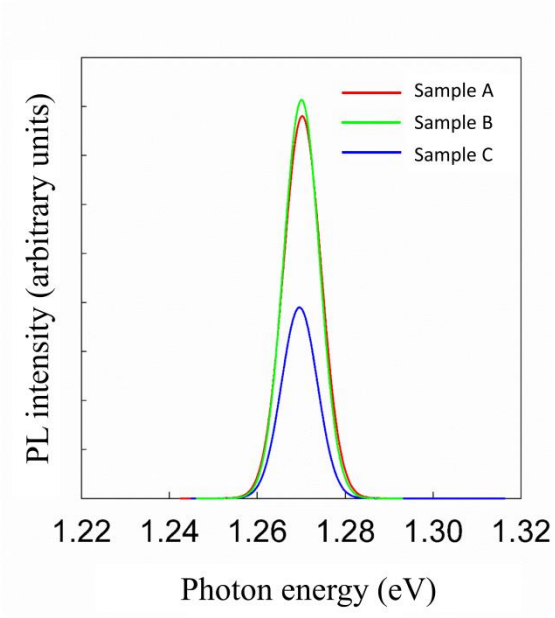

Figure 3.7 Room-temperature photoluminescence spectra of the samples.

No PL in the region of the GaAs band gap may indicate that the higher energy peaks are not from discrete levels in GaAs. To determine the line width of the PL peak, each PL spectrum was fitted by a Gaussian distribution function. The broadening in the PL peak is associated with an inhomogeneous nitrogen concentration in the structure [27]. The value of the line is estimated as 43, 41 and 42 meV for sample A, B and C, respectively. Although there is almost no difference the line width of the PL peak, the PL intensity of GaAsN increases significantly for sample A and sample B. This result demonstrates that the layer structure and the growth conditions of these samples make them suitable candidates for optical applications of $GaAs_{1-x}N_x$ (x~3%).

From the Equation 3.1 the ratio of N alloy concentrations can be calculated;

$$E_g(GaAs_{1-x}N_x) = x.E_g(GaN) + (1-x)E_g(GaAs) - bx(1-x) \qquad \textbf{(3.1)}$$

Eg: Band gap energy, eV

x: Alloy concentration ratio of N, %

b: Bowing parameter

3.4 Resistivity and Hall Effect Measurements

3.4.1 Resistivity measurement

For $GaAs_{1-x}N_x$ samples, resistivity and Hall effect measurements were implemented by using Van der Pauw technique. This technique requires four symmetric points on sample surface's four edge for contact. As it can be seen from the Figure 3.8 below for observing current-voltage alteration; only 4 measurements (2 resistivity and 2 Hall voltage) will be enough.

If we assume that $R_{12,34}$ is equal to R_A and $R_{23,41}$ is equal to R_B as stated in Equation 3.2

$$R_{12,34} = \frac{V_{34}}{I_{12}} = R_A \quad \text{and} \quad R_{23,41} = \frac{V_{41}}{I_{23}} = R_B \tag{3.2}$$

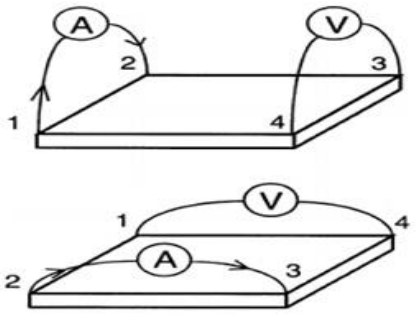

Figure 3.8 Resistivity measurement method of samples [28].

Resistivity was derived as below Equation 3.3 by Van der Pauw in 1958;

$$\rho = \left(\frac{\pi d}{ln2}\right) \frac{(R_{12,34}+R_{23,41})}{2} f\left(\frac{R_{12,34}}{R_{23,41}}\right) \tag{3.3}$$

d: Sample thickness

$R_{12,34}$: is the ratio of the current which is applied on contacts 1 and 2 to the voltage which occurs between the contact 3 and 4.

From the similar way, the current that pass through every contact pair will cause a voltage on the opposite pairs. The difference of voltage, which is manufactured by

the current that pass through pair of contacts, is applied to for 4 right direction current and 4 reverse direction current. Totally, we can obtain 8 resistivity measurements and take their average [29].

Also, we need to use correction factor of *f* as stated Equation 3.4 below,

$$f\left(\frac{R_{12,34}}{R_{23,41}}\right) = 1 - \left[\frac{(R_{12,34}-R_{23,41})}{(R_{12,34}+R_{23,41})}\right]^2 \frac{1}{2}\ln 2 - \left[\frac{(R_{12,34}-R_{23,41})}{(R_{12,34}+R_{23,41})}\right]^4 \left[\frac{(\ln 2)^2}{4} - \frac{(\ln 2)^3}{12}\right] \quad \textbf{(3.4)}$$

3.4.2 Hall effect measurement

If an electric current flows through a conductor in a magnetic field, the magnetic field exerts a transverse force on the moving charge carriers which tends to push them to one side of the conductor. This is most evident in a thin flat conductor as illustrated in Figure 3.9. A buildup of charge at the sides of the conductors will balance this magnetic influence, producing a measurable voltage between the two sides of the conductor. The presence of this measurable transverse voltage is called the Hall effect after Edwin Herbert Hall who discovered it in 1879 [30].

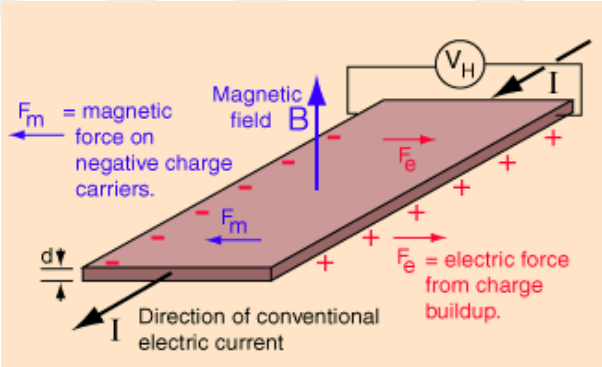

Figure 3.9 Schematic demostration of Hall effect [30].

The hole effect voltage is given by the Equation 3.5 as below;

$$V_H = \frac{IB}{ned} \quad \textbf{(3.5)}$$

n: density of mobile charges, cm^{-3}

e: electron charge, $1.602 \cdot 10^{-19}$ C

d: thickness of plate, cm

Generally Hall effect measurements are combined with the resistivity measurements and conventional system can be used. Magnetic field is applied to the surface vertically. Current is applied from one diagonal (cross) pair of contacts and from other diagonal contact pair, the voltage value can be observed. If we take the applied current unit is Amper, magnetic field is Gauss, thickness of sample is cm and observed voltage is Volt, coefficient of Hall can written as in Equation 3.6 below;

$$R_H = 10^8 \left[\frac{d\Delta R_{13,24}}{B}\right] \text{ cm}^3\text{C}^{-1} \quad \textbf{(3.6)}$$

Here, $\Delta R_{13,24}$ value is the change in resistance $R_{13,24}$ when magnetic field B is applied to sample vertically.

Similar to resistivity measurements by changing current direction and magnetic field direction we can find 8 different configurations of measurements.

As a conclusion, eight configuration from resistivity and eight configuration from Hall coefficient, totally sixteen configurations of measurements were performed.

Mobility of Hall μ_H and Hall carier concentration n_H can be written as below in the Equation 3.7 and 3.8 [29];

$$\mu_H = \frac{R_H}{\rho} \text{cm}^2(\text{V}^{-1})(\text{s}^{-1}) \quad \textbf{(3.7)}$$

$$n_H = \frac{1}{eR_H} \text{cm}^{-3} \quad \textbf{(3.8)}$$

In this thesis; Lakeshore 7700A High Impedance Hall effect system was used for attaining the mobility and carrier concentration values with respect to temperature. The main components and devices of this system are given in Figure 3.10 separately, on picture below.

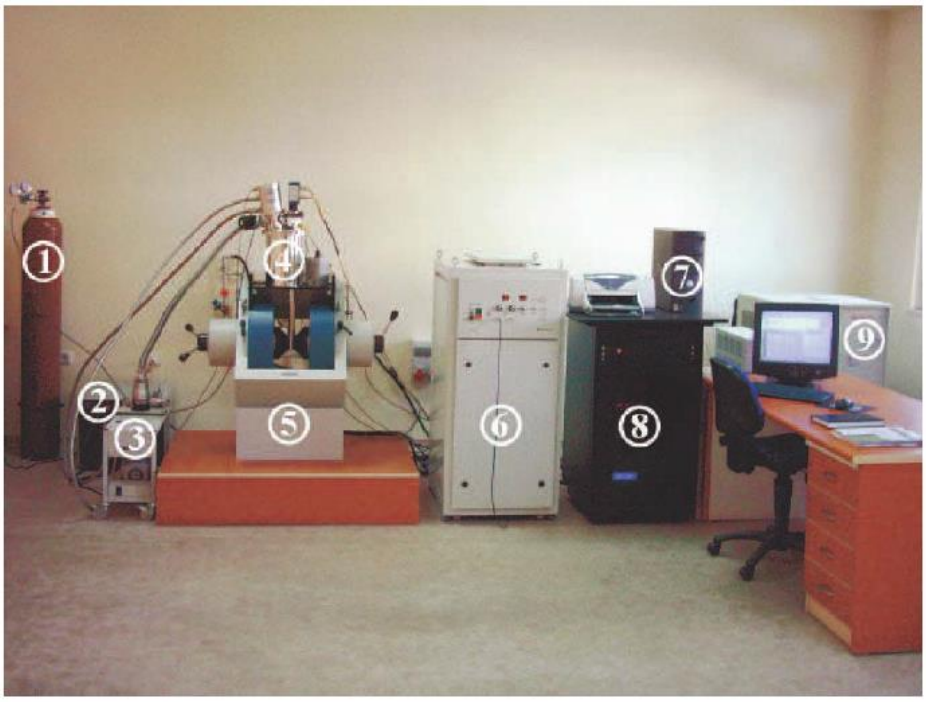

Figure 3.10 Lakeshore 7700A High Impedance Hall Effect System.

(1) Helium tube, (2) Closed circuit He cooling unit, (3) Vacuum pump, (4) Cryostat, (5) Magnet system, (6) Magnet power supply, (7) Computer, (8) Temperature control unit, Measurement instruments, Key system, Magnetic field measurement system (9) Water cooling system.

CHAPTER 4

RESULTS AND DISCUSSION

4.1 Temperature Dependent Mobility

Results show that mobility is thermally activated for samples A and B, and becomes weakly temperature dependent for sample C as it can be seen from the Figure 4.1. Hall effect analysis indicates that layer structures and growth conditions significantly affect GaAsN electron mobility.

The value of the electron mobility for sample B grown on GaAs-SI substrate was very high in comparison with other samples, and we should point out that the value of mobility for sample B ($3.3 \cdot 10^4 \frac{\mathrm{cm}^2}{\mathrm{V \cdot s}}$ at 40 K) is also significantly higher than those of GaAsN samples reported in the literature [31, 32]. On the other hand, incorporation of Si into GaAsN reduces the mobility of GaAsN layers grown on GaAs-SI substrate (see sample C). The sample A has the lowest mobility at room temperature. This might be due to increasing effective mass for this sample [33].

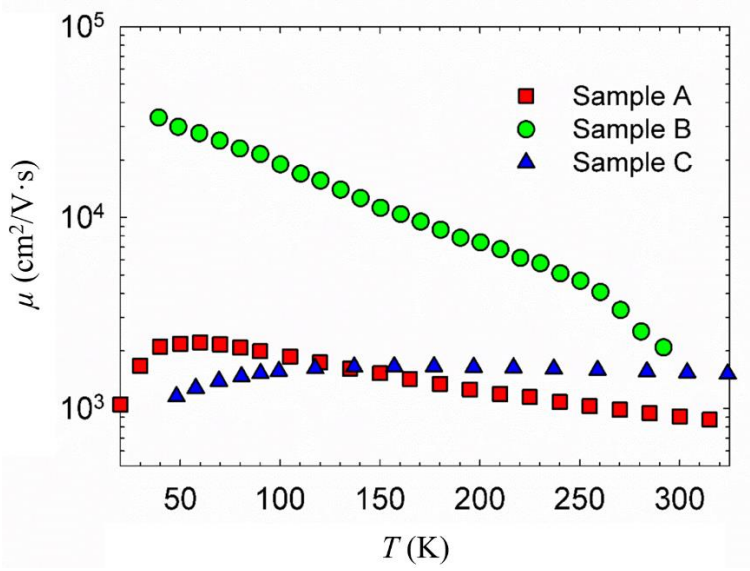

Figure 4.1 Mobility versus temperature.

4.2 Temperature Dependent Carrier Concentration

The carrier concentration data of sample A and sample C are flat over the whole temperature region, denoting a degenerate semiconductor behavior. To further validate that sample A and sample C exhibit degenerate semiconductor behavior, we consider critical concentration (n_c=(0.25/a_B)^3=1.8·10^{16} cm^{-3} for x = 3% in GaAs$_{1-x}$N$_x$, where a_B is Bohr radius) of carrier concentration given for the metal-insulator transition in Equation 4.1.

$$n_c = \left(\frac{0,25}{a_B^*}\right)^3 \tag{4.1}$$

$$a_B^* = \frac{\varepsilon_0 \varepsilon_r h^2}{\pi m^* q^2} \tag{4.2}$$

As seen from Figure 4.2 the carrier concentration values of sample A and sample C are greater than the critical concentration (n_c), which demonstrates that these two samples exhibit the degenerate semiconductor behavior. On the other hand, sample B, whose carrier concentration ($n < n_c$) thermally increases with rising temperature, falls on the insulating side of the metal-insulator transition region over the whole temperature range. A lower carrier concentration observed for sample B might be due to mobile carrier trapping at N interstitials [34].

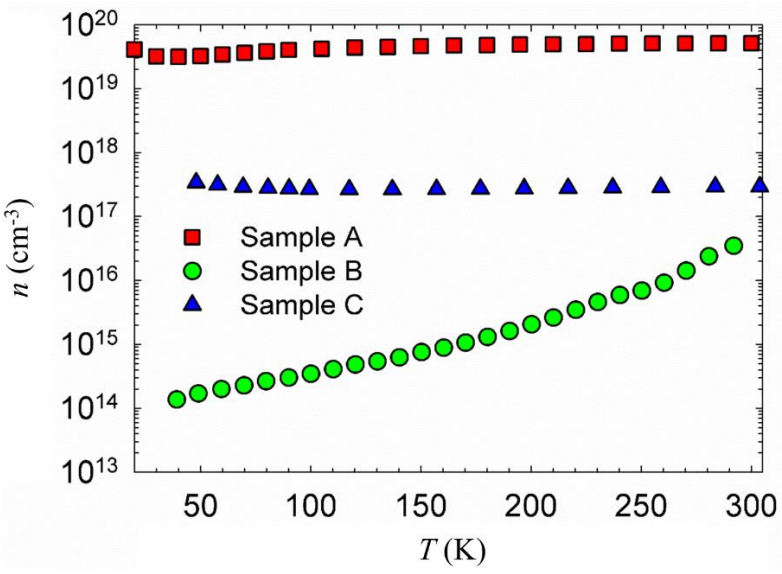

Figure 4.2 Temperature dependent carrier density of the samples.

4.3 Temperature Dependent Electrical Conductivity

The values which are measured and calculated for the samples A, B and C were given in Table 4.1 and used for calculation of electrical conductivity.

Table 4.1 Attained electrical results of $GaAs_{1-x}N_x$ samples at room temperature.

Sample	Concentration of N (%)	$\mu\ (\frac{cm^2}{V \cdot s})$	$n\ (cm^{-3})$	$\rho\ (\Omega \cdot cm)$	$\sigma = 1/\rho$
A	2.98	908.5	$5.15 \cdot 10^{19}$	$1.33 \cdot 10^{-4}$	7518.79
B	3.01	2090	$3.49 \cdot 10^{15}$	$8.55 \cdot 10^{-2}$	11.69
C	2.91	1538	$2.94 \cdot 10^{17}$	$1.38 \cdot 10^{-2}$	72.46

Figure 4.3 shows the temperature dependence of the conductivity ($\sigma = ne\mu$, where e is the electron charge) for the samples. It is obvious that sample B with lower carrier concentration exhibits insulator-like conductivity, while the conduction of other samples with higher carrier concentration appears metallic-like.

The weak temperature dependence of the conductivity for sample A and sample C is incorporated because of the weak temperature dependent observed from mobility and carrier concentration behavior.

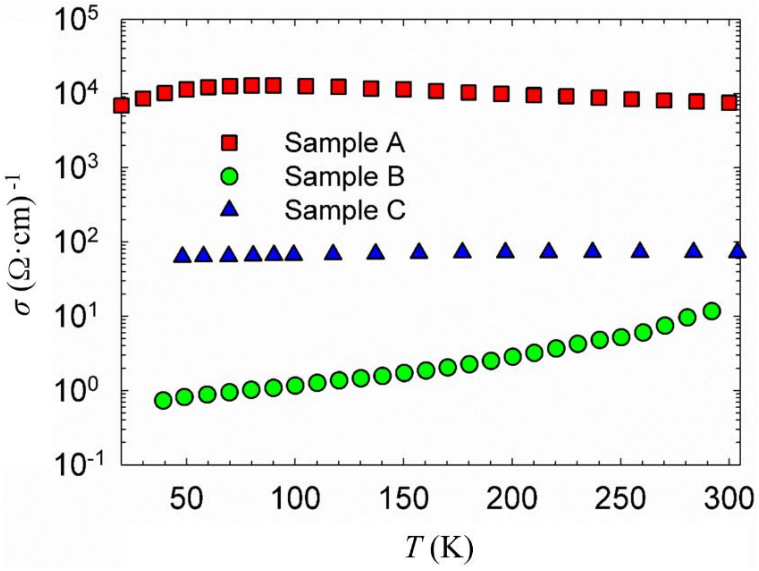

Figure 4.3 Change of electrical conductivity with temperature.

4.4 Temperature Dependent Power Factor

We finally investigated the power factor ($PF = S^2\sigma = S^2 ne\mu$). We already measured n and μ as a function of temperature. However, the Seebeck coefficient (S) was not directly measured, which could be used for comparison. On the other hand, the calculated values of S for both samples are very probable as we will see.

Based on the discussion above, we can see that the Seebeck coefficient of sample A and sample C can be calculated by a given relationship (4.3) between carrier concentration and Seebeck coefficient for degenerate semiconductors [35].

$$S = \frac{8\pi^2 k_B^2}{3eh^2} m^* T \left(\frac{\pi}{3n}\right)^{\frac{2}{3}} \quad \textbf{(4.3)}$$

where k_B is Boltzmann's constant, h is Planck's constant, m^* is effective mass of carriers, and n is the carrier concentration. Note that we are not able to calculate the Seebeck coefficient of sample B due to its non-degenerate behavior. It is expected that sample B has significantly low value of *PF*.

From Equation (4.3), it is apparent that the Seebeck coefficient increases according to the reduction in the carrier concentration. Actually; the estimated values of Seebeck coefficient for the samples with Equation (4.3) given in Table 4.2 are well consistent with the experimental findings for GaAsN [36, 37].

Combining these results with Hall effect results allows us to obtain the temperature dependence of the *PF* of sample A and sample C, as shown in Figure 4.4. The *PF* increases as temperature increases for both samples.

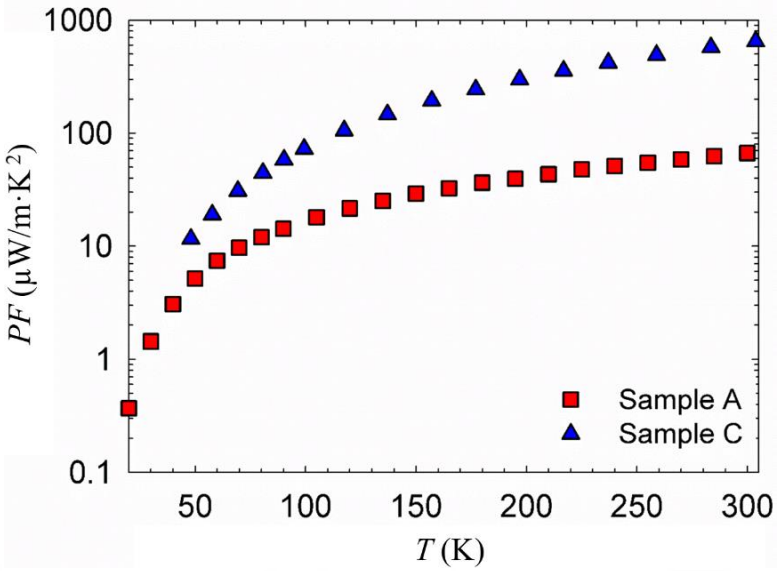

Figure 4.4 *PF* values dependent on temperature.

If we compare with sample A; sample C shows the larger *PF* value both at room temperature and at low temperature, owing to its relatively lower carrier concentration and sufficiently high conductivity. As seen from Table 4.2 below, room-temperature *PF* value of sample C is about 10 times larger than that calculated for sample A.

Since the nitrogen content is so close for the samples, we can consider layer structure and growth conditions of the samples for comparison. It is noteworthy that the thermoelectric properties for the GaAsN films are excellent with a GaAs-SI substrate and Si dopant.

Table 4.2 Obtained electrical properties of the samples and *PF* values.

Parameters	**Sample A**	**Sample B**	**Sample C**
x (%)	2.98	3.01	2.91
μ ($cm^2/(V{\cdot}s)$)	908.5	2090	1538
n (cm^{-3})	$5.15{\cdot}10^{19}$	$3.5{\cdot}10^{15}$	$2.94{\cdot}10^{17}$
σ $(\Omega{\cdot}cm)^{-1}$	7518.79	11.69	72.46
S (μV/K)	−9.4 (5 ~ 20*)	-	−298 (280 ~ 320*)
PF ($\mu W/(m{\cdot}K^2)$)	66	-	648

* The experimental values taken from literature for comparing [36, 37].

CHAPTER 5

CONCLUSION

In this thesis; experimental and theoretical investigation of thermoelectric efficiency of Si doped GaAsN material was studied. By changing the substrates and alloy of the samples; different electrical, optical and thermoelectric properties were obtained. *ZT* value of materials, which is function of the Seebeck coefficient, electrical conductivity and thermal conductivity, was evaluated as an indicator of thermoelectric efficiency of materials.

For derivation of *ZT* value; basic thermodynamic and thermoelectric concepts like Carnot cycle efficiency, Seebeck effect, Peltier effect and Thomson effect were taken into consideration.

GaAsN samples were fabricated by MOVPE on SI (semi-insulating) and n-type GaAs substrates. The nitrogen content of the samples was around 3%. A systematic investigation was performed dependence of optical, electrical and thermoelectric properties on layer structure and growth condition of the samples.

Sample A exhibited a degenerated semiconductor behavior which was growth on n-type GaAs substrate. Even if, it shows the highest carrier concentration value among the other samples; the mobility value of sample A at room temperature was too low. By considering that the mobility value of sample A must be improved for attaining a higher *ZT*, the substrate changed in sample B as SI-GaAs.

After changing the substrate as SI-GaAs in sample B, it was observed that mobility is developed significantly. Nonetheless, carrier concentration value of sample B was not promising as a candidate of thermoelectric device. Carrier concentration value of sample B was under the critical number which is called critical carrier concentration level.

Eventually; without changing the SI-GaAs substrate structure, Si doping process into GaAsN was executed for enhancing *PF* value in sample C. Even though sample C has a lower value of electrical conductivity compared with sample A, it has higher Seebeck coefficient then sample A.

Sample B exhibited the largest PL intensity and it has the highest mobility among others, those make it eligible for optoelectronic applications of GaAsN. Sample A and sample C showed a degenerate semiconductor behavior which is desired for thermoelectric applications.

Finally, the *PF* value of GaAsN was remarkably improved with Si doping as seen sample C. This conclusion indicates that the layer structure and growth conditions are very important for both material structure quality and possible device performance of GaAsN as a thermoelectric material. Therefore, the layer structure and growth conditions of sample C might be considered the ideal ones for further investigation of thermoelectric properties of GaAsN.

REFERENCES

[1] Kedsongpandlya, S., Nanolaminated Thin Films for Thermoelectrics, Master Thesis, Department of Physics/Chemistry and Biology, Linköping University, Linköping, Sweden, 2010.

[2] Kedsongpandlya, S., Design of Transition-Metal Nitride Thin Films for Thermoelectrics, Ph. D Thesis, Department of Physics/Chemistry and Biology, Linköping University, Linköping, Sweden, 2015.

[3] Zhang, X. and Zhao, L., Thermoelectric materials: Energy Conversion Between Heat and Electricity, Journal of Materiomics, 92-105, 2015.

[4] Hou, Q. R., Gu, B. F., Chen, Y. B. and He, Y. J., Enhancement of thermoelectric power factor of $MnSi_{1.7}$ films by Si addition and modulation doping, Phys. Status Solidi A, 1-6, Department of Physics, Tsinghua University, Beijing, China, 2012.

[5] Yamaguchi, M., Paek J., Amano, H., Thermoelectric Power Measurement of Catalyst-free Si-doped GaAs Nanowires, Materials Research Society, 1439, 83-87, 2012.

[6] Zou, X., Chen X., Huang, H., Xu Y., Duan, W., Enhanced Thermoelectric Figure of Merit in Thin GaAs Nanowires, Nanoscale, 2015.

[7] Reshak, A.H., Thermoelectric properties of highly mismatched alloys of GaN_xAs_{1-x} from first to second principles methods: energy conversion, RSC Advances, 6, 72286-72294, 2016.

[8] Ohta, S., Nomura, T., Ohta, H and Koumoto, K., High-temperature carrier transport and thermoelectric properties of heavily La or Nb doped $SrTiO_3$ single crystals, Journal of Applıed Physıcs 97, 034106, Nagoya University, Graduate School of Engineering, Nagoya Japan, 2005.

[9] Lin, S., Why the heat powered stove fan can run without electric, 7th April 2016 www.linkedin.com, [Access date: September 2017].

[10] Jeffrey, S. G. and Toberer, E. S., Complex Thermoelectric Materials, Nature Materials 7, 105-114, 2008.

[11] Paul, D., ICT Energy Concepts Towards Zero Power Information and Communication Technology, Chapter 4. Thermoelectric Energy Harvesting, Intech, 2014.

[12] Goldsmid, H. J., Conversion Efficiency and Figure-of-Merit, Chapter 3, Florida CRC, 1995.

[13] Conductivity of Semiconductor, 2012-2017, http://www.electrical4u.com, [Access date: October 2017].

[14] Turton, R. J., The Physics of Solid, Oxford, 2000.

[15] What are ceramics, Science Learning Hub, www.sciencelearn.org.nz, 2010. [Access date: November 2017].

[16] Wunderlich, W. and Baufeld, B., Ceramic Materials, Chapter 1: Development of Thermoelectric Materials Based on NaTaO3 Composite Ceramics, Intech Publisher, pp.1-27, 2010.

[17] Koumoto, K., Funahashi, R., Guilmeau, E., Miyazaki, Y. Weidenkaff, A., Wang, Y., and Wan, C., Thermoelectric Ceramics for Energy Harvesting, The American Ceramic Society 96, 1-23, 2013.

[18] Dubey, N. and Leclerc, M., Conducting Polymers: Efficient Thermoelectric Materials, Polymer Physics 49, 467-475, 2011.

[19] Herres, D., Why Silicon and Germanium are Semiconductors [online], WTWH Media LLC, 2016, www.testandmeasurementtips.com, [Access date: November 2017].

[20] Zheng, J. C., Recent Advances on Thermoelectric Materials, Front. Phys. China, 3(3), 269-279, 2008.

[21] www.wikipedia.org, [Access date: October 2017].

[22] www.saha.ac.in, 17th August 2016, [Access date: December 2017].

[23] www.ims.uconn.edu, [Access date: December 2017].

[24] Kim, T.S., Cuong, T.V., Park, C.S., Park, J.Y., Lee, H.J., Suh, E.K., Hong, C.H., Composition Dependence of the Band-gap Energy of GaAsN Alloys, Journal of Korean Physical Society 43, 273, 2003.

[25] www.archive.cnx.org, [Access date: July 2017].

[26] www.wikipedia.org, [Access date: July 2017].

[27] Uesugi, K., Suemune, I., Hasegawa, T., Akutagawa, T., Nakamura, T., Temperature Dependence of Band gap Energies of GaAsN Alloys, Applied Physics Letters, 76, 1285-1287, 2000.

[28] www.researchgate.net, [Access date: September 2017].

[29] Yıldız, A., $In_xGa_{1-x}N$ Yarıiletkenin Elektron İletim Özellikleri, Ph. D Thesis, Gazi University, Institute of Science, Ankara, 2008.

[30] www.hyperphysics.phy-astr.gsu.edu, [Access date: June 2017].

[31] Moto, A., Tanaka, S., Ikoma, N., Tanabe, T., Takagishi, S., Takagishi, M., Katsuyama, T., Metalorganic Vapor Phase Epitaxial Growth of GaAsN Using Tertiarybutylarsine (TBA) and Dimethylhydrazine (DMHy), Japanese Journal of Applied Physics, 38, 1015, 1999.

[32] Young, D. L., Geisz, J. F., Coutts, T. J., Nitrogen-induced Decrease of the Electron Effective Mass in $GaAs_{1-x}N_x$ Thin Films Measured by Thermomagnetic Transport Phenomena, Applied Physics Letters, 82, 1236-1238, 2003.

[33] Eber, F., Drachenko, O., Patane, A., Ozerov, M., Winnerl, S., Schneider, H., Helm, M., Direct Determination of the Electron Effective Mass of GaAsN by Terahertz Cyclotron Resonance Spectroscopy, Applied Physics Letters, 107, 062103, 2015.

[34] Reason, M., McKay, H. A., Ye, W., Hanson, S., Goldman, R. S., Rotberg, V., Mechanisms of Nitrogen İncorporation in GaAsN Alloys, Applied Physics Letters, 85, 1692-1694, 2004.

[35] Cutler, M., Leavy, J. F., Fitzpatrick, R. L., Electronic Transport in Semi-metallic Cerium Sulfide, Physical Review, 133, A1143, 1964.

[36] Pichanusakorn, P., Kuang, Y. J., Patel, C. J., Tu, C.W., Bandaru, P. R., The İnfluence of Dopant Type and Carrier Concentration on the Effective Mass and Seebeck Coefficient of $GaAs_{1-x}N_x$ thin films, Applied Physics Letters, 99, 072114, 2011.

[37] Dannecker, T., Jin, Y., Cheng, H., Gorman, C. F., Buckeridge, J., Uher, C., Fahy, S., Kurdak, C., Goldman, R. S., Nitrogen Composition Dependence of Electron Effective Mass in $GaAs_{1-x}N_x$. Physical Review B, 82, 125203, 2010.

CURRICULUM VITAE

PERSONAL INFORMATION

Name Surname : Yusuf YILDIZ

Date of Birth : 1988

Phone : +90 506 562 52 32

E-mail : yusuf.yildiz@tai.com.tr

yusufyildiz88@hotmail.com

EDUCATION

High School : Süleyman DEMİREL Anatolian High School/ANKARA (4.18/5.00) (2002-2006)

Bachelor : Gazi University, Engineering Faculty, Mechanical Engineering Department/ANKARA (2007-2012) (2.94/4.00)

Master Degree : Ankara Yıldırım Beyazıt University, Institute of Natural Sciences, Mechanical Engineering Department/ANKARA (2013-continued)

WORK EXPERIENCE

Field Chief : Osman Oğulları İnşaat (2013-2014)

Field Chief : TACE Mühendislik (2015)

Subcontract Administrator : TAI-Turkish Aerospace Industry/ANKARA (2015-continued)

TOPICS OF INTEREST

Energy, Thermodynamics, Solar energy, Heat transfer, Thermoelectric energy.

PUBLICATIONS SCI (Under Review)

Yıldız, Y., Bilen, K., Yıldız, A., Bosi, M., The thermoelectric power factor enhancement of $GaAs_{1-x}N_x$, Journal of Optoelectronics and Advanced Materials.

CONFERENCE (Oral Presentation)

The Effect of Si on Thermoelectric Efficiency of GaAsN Alloys, Turkish Physical Society 33rd International Physics Congress, Bodrum/TURKEY, September 6-10, 2017.